

Article

Effects of Rain and Sediment-Laden Winds on Earthen Archaeological Sites from Morphometry: A Case Study from Huaca Chotuna (8th–16th Century AD), Lambayeque, Peru

Luigi Magnini ¹, Maria Iliaria Pannaccione Apa ², Robert F. Gutierrez Cachay ³, Marco Fernández Manayalle ⁴, Carlos E. Wester La Torre ⁵ and Guido Ventura ^{2,6,*}

¹ Dipartimento Di Studi Umanistici, Università Ca' Foscari Venezia, Fondamenta del Malcanton, 30100 Venezia, Italy; luigi.magnini@unive.it

² Istituto Nazionale di Geofisica e Vulcanologia, Via di Vigna Murata 605, 00143 Roma, Italy; mariailaria.pannaccioneapa@ingv.it

³ Museo Arqueológico Nacional Brüning, Huamachuco, Lambayeque 14013, Peru; robert1905.rgc@gmail.com

⁴ Museo de Sitio Huaca Chotuna-Chornancap, San Martín-San José, Lambayeque 14013, Peru; marcofer23@yahoo.es

⁵ Dirección Desconcentrada de Cultura de Lambayeque y Dirección Ejecutiva de la Unidad Ejecutora 005 Naylamp Lambayeque, Avenida Luis Gonzáles 345, Chiclayo 14000, Peru; carloswesterlatorre2000@yahoo.es

⁶ Istituto di Scienze Marine, Consiglio Nazionale delle Ricerche, Calata Porta di Massa, 80133 Napoli, Italy

* Correspondence: guido.ventura@ingv.it; Tel.: +39-06-51860221

Abstract

Earthen archaeological sites are particularly vulnerable to rain and winds, whose effects may compromise their integrity. The Huaca Chotuna (HC; 8th–16th Century AD) is an adobe platform in Peru's semi-arid Lambayeque region, and it is in an area with exposure to rain and winds associated with the El Niño Southern Oscillation (ENSO) events. Here we present the results from an orthophotogrammetric and morphometric study aimed at quantifying the effects of erosion and deposition at the HC. The novelty of our approach consists of merging topographic, hydrological, and wind parameters to recognize the sector of the HC with exposure to potentially damaging natural climatic phenomena. We identify zones affected by erosion and deposition processes. Results of a diffusion model aimed to estimate the HC sectors where these processes will act in the next century are also presented. Gully erosion from rainfall indicates a vertical erosion rate of approximately 0.2 m/century, demonstrating the low preservation potential of the HC. Rainwater also deteriorates adobe bricks and triggers water/mud flows. Conversely, sediment-laden winds contribute to the partial burial of the HC. The findings highlight significant hazards to the HC's structural integrity, including gravity instability. The interdisciplinary methodology we adopt offers a key framework for assessing and protecting other earthen sites globally against the escalating impacts of climate change.

Keywords: earthen archaeological site; preservation; digital morphometry; climatic vulnerability; hazard



Academic Editors: Lorenzo Teppati Losè, Elisabetta Colucci and Arnadi Dhestaratri Murtiyoso

Received: 20 July 2025

Revised: 4 September 2025

Accepted: 4 September 2025

Published: 5 September 2025

Citation: Magnini, L.; Apa, M.I.P.; Gutierrez Cachay, R.F.; Manayalle, M.F.; La Torre, C.E.W.; Ventura, G. Effects of Rain and Sediment-Laden Winds on Earthen Archaeological Sites from Morphometry: A Case Study from Huaca Chotuna (8th–16th Century AD), Lambayeque, Peru. *Remote Sens.* **2025**, *17*, 3103. <https://doi.org/10.3390/rs17173103>

Copyright: © 2025 by the authors. Licensee MDPI, Basel, Switzerland. This article is an open access article distributed under the terms and conditions of the Creative Commons Attribution (CC BY) license (<https://creativecommons.org/licenses/by/4.0/>).

1. Introduction

Erosion due to rainfall and wind represents a key environmental process affecting the Earth's surface. Effects of erosion include changes in the properties and distribution of soils, groundwater recharge/discharge cycles, stream network geometry, and damage to the infrastructures of urban, transportation and agricultural areas, and to cultural

heritage [1–3]. Among the different factors controlling the intensity of erosion processes, the increasing amount of rainfall intensity and strong winds related to climate change play a major role [4,5], being that rainfall intensity is proportional to erosion rate [6,7]. In such a perspective, erosion poses a serious threat to cultural heritage [8–10]. Water and winds are cause of the loss of structural integrity of the pre-Hispanic settlements, especially those affected by potentially dangerous climatic phenomena as the El Niño Southern Oscillation (ENSO) events [11,12]. Therefore, the conservation of such sites needs a clear understanding of the erosion processes and their relations with climate [13,14]. Defending cultural heritage requires an interdisciplinary approach including monitoring and hazard evaluation in the framework of climate adaptation plans, conservation actions, and sustainable land use [15–18]. However, the first step in the evaluation of the preservation strategies is the recognition of the connections between erosion processes and induced degradation. About 10% of the world’s heritage consists of earthen sites often affected by erosion due to intense rainfall, wind, and sediment-laden wind [19,20]. Archaeological sites located along the northern coast of Peru in the Lambayeque region mainly consist of platforms (huacas, from the Quechuan wak’a) made up of adobe (clay–silt–straw bricks). These peculiar ceremonial buildings date from the 2nd Millenium BC to the 16th Century AD [21–23]. The Complejo Arqueológico Chotuna-Chornancap (Chotuna-Chornancap Archaeological Complex; Figure 1a,b) is an important ceremonial center including truncated pyramid-shaped structures developed in the Lambayeque valley from the 6th to 7th Century AD until the time of the annexation by the Tawantinsuyu (Inca Empire) in the 5th Century AD. The main huacas of the Lambayeque coastal area also include Tucume, Mirador, Colluz, and Soternic (Figure 1a,b). This area is characterized by a semi-arid climate, and the bedrock on which the huacas are located consists of lacustrine, alluvial, and aeolian deposits (dunes) [24]. Between May and January–February, the Lambayeque region is affected by south-directed winds related to the Humboldt current [25], whereas west-directed winds related to the ENSO events concentrate between February and April. The timing of El Niño can be roughly predicted but the associated rain and wind intensity remains difficult to forecast [26]. The frequency of the extreme ENSO is expected to increase in the future due to climate change [27]. Destructive ENSO events were recorded in sediments [28], and their impact on the northern coast of Peru date back to thousands of years ago [23,29]. In historical times, Ortloff and Kolata [30] showed that ancient irrigation systems and settlements in Lambayeque were repeatedly eroded, and the local communities rebuilt the infrastructure multiple times or relocated settlements [31].

According to [32], sediments and erosional truncation of floors found in archaeological sites containing 400 AD to 1400 AD old Moche and Chimu ceramics are related to destructive ENSO episodes. The stratigraphic features of these sites evidence the restoration activities of damaged structures. Also, the ENSO events that occurred between about 100 AD and 700 AD at Lambayeque are believed to be responsible for the agricultural collapse and the subsequent decline in Moche culture [33]. The more recent events (1925, 1982, 1997, and 2023) are well documented with clear evidence of heavy social and environmental impacts with destruction of agricultural, urban, and infrastructural settlements [34–37].

Here we present a study on the effects of rain and wind at the Huaca Chotuna (HC), the largest truncated pyramid of the Chotuna-Chornancap Archaeological Complex (Figure 1b–d). We combine field observations and results of an orthophotogrammetric survey carried out to obtain a high-resolution digital surface model (DSM) of the HC. The aim of our study is to (a) recognize the erosion and deposition features affecting the HC, (b) quantify the damages related to winds and/or rain from a morphometric analysis of a DSM, (c) provide an estimate of the present-day degree of preservation of the remaining structure, and (d) identify the HC sectors with a potential exposure to erosion or deposition due to

diffusion processes in the next century. Our analytical and operational approach, which combines archaeological, geomorphological, and morphometric data, provides a new operating framework that can be exported to other earthen settlements sites. The ultimate objective is to quantify the effects of climatic phenomena like rain and wind on earthen heritage. This objective represents a prerequisite to design preservation strategies and protection actions. With respect to other studies aimed at evaluating the effects of climatic phenomena on earthen heritage [8,9,13,14,18], we show how remotely acquired data are suitable for the estimate of sectors of archaeological sites affected by erosion and deposition processes associated with climatic phenomena.

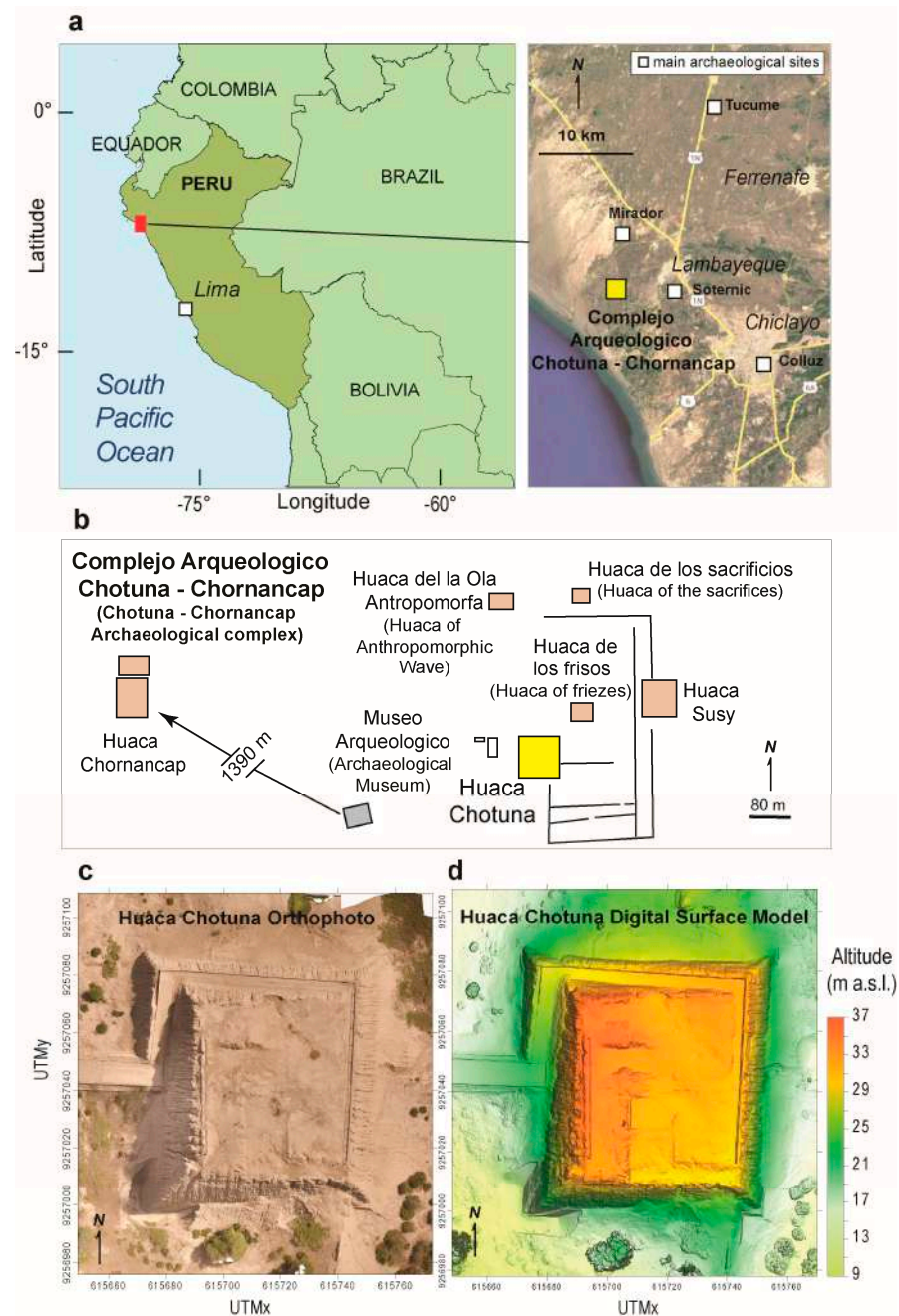


Figure 1. (a) Location map of the Complejo Arqueológico Chotuna-Chornancap and huacas of the Lambayeque region. Names of cities are reported italic character. (b) Map of the Complejo Arqueológico Chotuna-Chornancap with location of the Huaca Chotuna (yellow). (c) Orthophoto of the Huaca Chotuna; (d) digital surface model (DSM) of the Huaca Chotuna.

2. Historical and Archaeological Setting

The first written references on the Lambayeque area come from Spanish chroniclers including Francisco López de Xerez [38], Pedro Cieza de León [39], Miguel Cabello Balboa [40], Francisco Alcocer [41], and Garcilazo de la Vega [42]. The Lambayeque culture can be described as a complex society with a decentralized state composed of several family nuclei constituted as political entities based on ceremonial and administrative centers strategically located in the valleys [43–45]. Numerous ceremonial centers were erected, and the Chotuna-Chornancap Archaeological Complex is one of the most important and wide. This complex is located on a plain extending over an area of approximately 95 hectares. The surface is made up of migrating and stable, vegetated dunes, some of which partially cover important architectural structures. Some dunes have completely buried smaller buildings or architectural elements [46]. The Chotuna-Chornancap Archaeological Complex includes the main huacas HC and Chornancap, and other smaller buildings such as Huaca de los Frisos, Huaca Susy, Huaca de los Sacrificios, Huaca Antropomorpha, and minor enclosures (Figure 1b). These constructions were largely modified between 8th and 12th Century AD [47] and show clear evidence of erosion due to rainfall and burial due to the deposition of sand by sediment-laden winds [48]. The HC covers an area of about 6400 m². It is a magnificent architectural structure in the shape of a platform with a truncated pyramid-like development separated by urban and residential areas, some of which are buried by sand dunes. Brüning [49] analyzed the legend of Naymlap, the mythical ancestor and founder of the Lambayeque culture based on pre-Hispanic relics, and Kroeber [50] conducted the first systematic archaeological fieldwork. The HC is made up of adobe bricks (raw clay, silt, and straw) belonging to three construction phases, which can be identified from the different shapes of adobe bricks. These phases are [22] the Archaic Lambayeque (early phase: flat rectangular adobe, 8th–early 12th Century AD), Classic Lambayeque (middle phase: loaf adobe, late 12th–14th Century AD), and Late Lambayeque, Chimú-Inca and Inca (late phase: loaf-shaped adobe, late 14th–16th Century AD). In a plane view, the HC is a square and the present-day height is 26 m but, based on the constructions found below the surface and those at the top in historical times, the original height may have been in the order of 40 m [22]. The construction phase currently exposed is that ascribable to the Classic Lambayeque period (Wester La Torre, 2010; 2011) [46,47]. The HC has an access ramp running at the base orthogonally to the western side and parallelly to the western and northern sides moving toward the top. The HC top is constituted by relics of enclosures [22,48]. To the west, at the base of the HC, excavations have returned architectural remains of rectangular courtyards with access to the north, probably dedicated to artisanal and specialized activities. A large enclosure interpreted as a main plaza enclosed by poorly preserved walls and dedicated to ceremonial and administrative activities occurs at the top of the HC [22]. The Chotuna-Chornancap Site Museum was inaugurated in 2009, exhibiting artifacts and human remains from the rich pre-Hispanic history of the Lambayeque region and Peru's northern coast.

3. Methods

A field survey has been carried out with the aim of recognizing the type of sediments surrounding and partially covering the HC and the construction materials(s) of the architectural structure. Also, this survey allowed us to plan the flight path for the orthophotogrammetric acquisition, which was carried out along 6 to 12 m spaced E-W and N-S striking stripes.

3.1. Orthophotogrammetry and DSM

An orthophotogrammetric survey of the HC was carried out on 2 May 2025, a sunny day with a wind velocity of <8 km/h from SW. The acquisition technique and the analytical methods are detailed in [51]. We used a UAV quadcopter, DJI Inspire 1.0, with a camera, Zenmuse X3 (sensor CMOS 1/2.3; resolution 12 megapixel). The UAV includes a navigation system (GNSS, gyroscopes, altimeter, and magnetic compass). The flight has been carried out at an altitude of 20 ± 2 m above ground. The camera angle varied between the vertical and 32° from the vertical; this latter angle has been set to acquire detailed images of the steeper slopes characterizing the HC outer flanks. A total of 493 12-megapixel images were acquired with 72–84% overlapping. The UAV and a base station have been interconnected by standard data radio communication and the data recorded in UTM coordinates (WGS84), zone 17S. Ten control points constituted by pre-marked targets have been measured before the survey with a Trimble R6 GPS Receiver in Real-Time Kinematic mode. We obtained horizontal coordinates of such control points with a Root Mean Square Error (RMSE) of 1 cm on x and y and 3 cm on z. The photogrammetric 3D reconstruction of EMLAC has been carried out with the AgisoftPhotoScan Professional Edition software (v. 1.7.4; <https://www.agisoft.com>) and a digital surface model (DSM) has been created using the Surfer software (v. 20.1.195) by GoldenSoftware. The orthoimages include the planimetric (x,y) data and the DSM the elevation (z). The acquired images have a resolution of 6 cm/pixel with an accuracy of 4.5 cm. The DSM of the HC has a resolution of 9 cm/px with an estimated RSME of 5 cm on x and y and 7 cm on z. The orthophoto and DSM are reported in Figure 1.

3.2. Morphometric Parameters

The morphometric parameters we compute from the DSM have been selected with the aim to characterize the morphological structure of the HC and analyze the effects of rainfall and winds on the architectural layout. Also, we employ a hillslope diffusion model to identify the sectors of the HC subjected to erosion or deposition related to diffusive processes such as soil creep, rain splash, and discontinuous surface runoff [52,53]. The morphometric parameters are defined below and include the following:

- Aspect, which is the azimuth that a terrain surface faces. Aspect is measured in degrees from the North in a clockwise trend following [54]:

$$\text{Aspect} = 270 - 360/2\pi \operatorname{atan} 2 [(Z_N - Z_S)/2\Delta y, (Z_E - Z_W)/2\Delta x] \quad (1)$$

where Z is the vertical component, x and y the horizontal components, and the subscripts N, S, E, and W the cardinal points.

- Slope is measured in degrees according to [54]:

$$\text{Slope} = 360/2\pi \arctan \sqrt{[(Z_E - Z_W)/2\Delta x]^2 + [(Z_N - Z_S)/2\Delta y]^2} \quad (2)$$

- Topographic Wetness Index (TWI). We use this parameter to identify the areas where the water may flow and accumulate during rain events [55]. TWI is a dimensionless parameter used in hydrological analysis defining the balance of the catchment water supply and local drainage. TWI provides information on the potential runoff generation, and its determination requires two input parameters [56]: the local upslope area draining through a certain point per unit contour length A, and the local slope S in radians. The analytical expression is:

$$\text{TWI} = \ln[(A)/\tan(S)] \quad (3)$$

- Stream network and watershed basins have been determined following [57] as implemented in [58]. The Strahler order of the stream network, i.e., the hierarchy of streams,

has been calculated with the MATLAB R2024a routine Strahler Stream by Wolfgang Schwangharta available online at <https://www.mathworks.com/matlabcentral/fileexchange/22952-strahler-stream-order> (accessed on 15 May 2025).

- Overland flow horizontal distance (O_f). O_f is related to the movement of water on the surface towards its confluence, termed the outlet [59], and the values have an inverse relation with the drainage density of the watershed being the lower O_f value, the higher the travel time of the runoff. O_f is defined as follows [59]:

$$O_f = 1/2D_d \quad (4)$$

with

$$D_d = L_u/A_w \quad (5)$$

where D_d is the drainage density, L_u is the stream length, and A_w is the watershed area. We determine the overland flow with the flow algorithm by [60].

- Wind Effect Index. We determine the extent and degree of upwind or downwind exposure of the HC by calculating the Wind Effect Index (WEI), which is a dimensionless index [61]. Values of WEI < 1 indicate the areas shielded from the wind, whereas values > 1 indicate areas exposed to wind. For the calculation of WEI, we follow the algorithm proposed by [61]. The Wind Effect index is the product of the windward and leeward indexes. These indexes are calculated considering the horizontal distances in windward and leeward directions and the corresponding vertical distances compared with the considered raster cell. The required input parameters are the prevailing wind direction and the digital topography of the study area. To measure the exposure of the HC to the wind, we adopt two prevailing wind directions: (a) a 180°N (from South) wind, which is the principal yearly direction along the Lambayeque coast of Peru [62], as above reported; and (b) a 270°N (from West) wind due to the El Niño episodes in March–April along the northern coast of Peru [36]. The above selected directions also characterize the HC area according with meteorological data from the Capitán FAP José A. Quiñones González International Airport at Chiclayo and Servicio Nacional de Meteorología e Hidrología del Perú (<https://www.gob.pe/senamhi>, accessed on 10 May 2025).
- Hillslope diffusion model. To have a semi-quantitative estimate of the areas of potential deposition and erosion due to diffusive processes, we use a hillslope evolution model based on the following equation [53]:

$$\delta h/\delta t = D\delta^2 h \delta x^2 + \delta^2 h \delta y^2 \quad (6)$$

where D is the diffusion coefficient, h is the height, t is time, and x and y are the spatial dimensions. Because of the semi-arid climate of the Lambayeque region and the clay-dominated HC constructive elements, we adopt $D = 360 \times 10^{-4} \text{ m}^2/\text{yr}$ [52,63] and perform the calculation over a time of 1 century. To highlight the effects of diffusive processes on HC and identify the areas affected by erosion or deposition, we compute the difference in altitude between the measured DSM of the HC and that computed by applying Equation (6) to such a DSM.

In determining the spatial distribution of the values of the above defined morphometric parameters we exclude from the DSM all the areas covered by vegetation. To achieve this, we analyze the orthophoto (Figure 1c) to delineate the vegetated areas with polygons. Then, we remove the pixels within the polygons from the DSM.

4. Results

4.1. Deposits, Sedimentary Structures, and Morphologies Related to Anthropogenic Activity

The results of the field and photogrammetric survey of the HC are summarized in Figure 1c,d, Figures 2–4. Data from Figure 1c,d and Figure 2a show that the HC has a square plan with sides measuring about 80 m. Its present-day maximum elevation is 37 m a.s.l. and the effective height is about 26 m. The lower flanks of the HC consist of sandy to silty sediments fully covering the base of the structure and about half of its original flanks (Figure 2a).

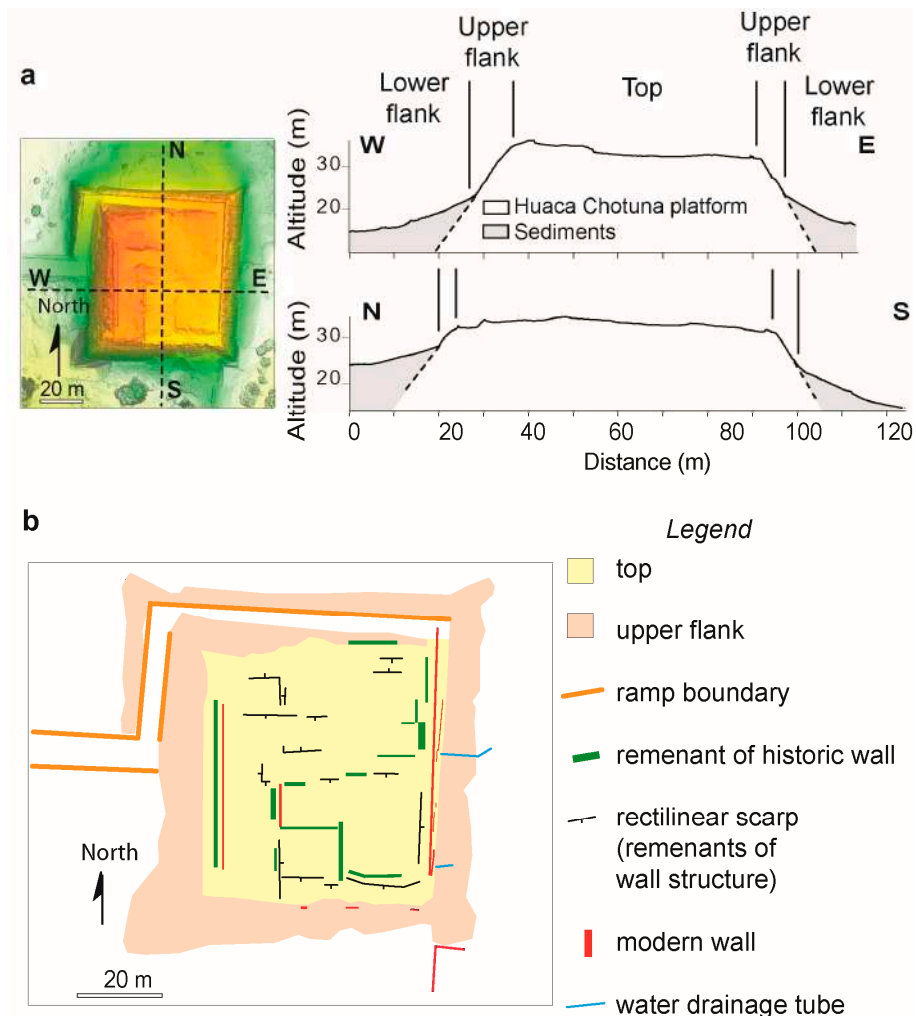


Figure 2. (a) DSM of Huaca Chotuna with trace of the cross sections reported on the left. Color scale as in Figure 1d (b) Architectural map of the Huaca Chotuna obtained by combining information from the orthophoto, DSM, and field survey.

The steeper upper flanks, which represent the original HC flanks, consist of clay-rich adobe bricks covered by massive, unstructured clay-rich sediments. The top of the HC is nearly flat and characterized by remnants of walls and scarps delimiting original enclosure structures (Figure 2b). Modern walls are also present. These have been constructed to regiment the water flow during rain episodes. The access ramp has been reconstructed in recent times, and, at the present, it is laterally delimited by two cm-high rows of bricks. Figure 3 shows that the core of the HC is made up of relatively preserved, loaf- to tall loaf-shaped bricks (Figure 3a,b). The few bricks outcropping on the HC upper flanks are heavily deteriorated and partially dismantled (Figure 3c,d). In addition, they are often covered by a clay-rich patina (Figure 3c) derived from the melting/dissolution of the underlying

bricks. Some bricks show mm-sized nearly parallel to anatomizing incisions reflecting the action of water and dehydration cracks associated with thermal stress due to the semi-arid climate of the area (Figure 3d).

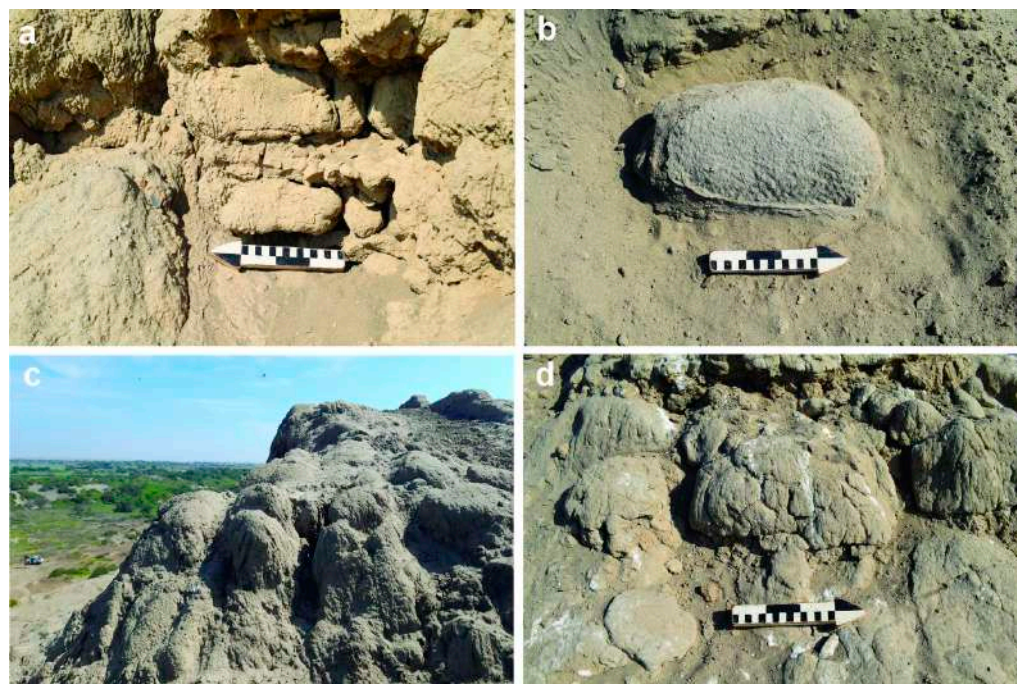


Figure 3. (a,b) Photos of preserved adobe bricks of the Huaca Chotuna (scale bar is 15 cm). (c) Partially preserved adobe bricks covered by a clay-rich patina. (d) Poorly preserved adobe bricks with dehydration fractures and smooth surfaces due to runoff.

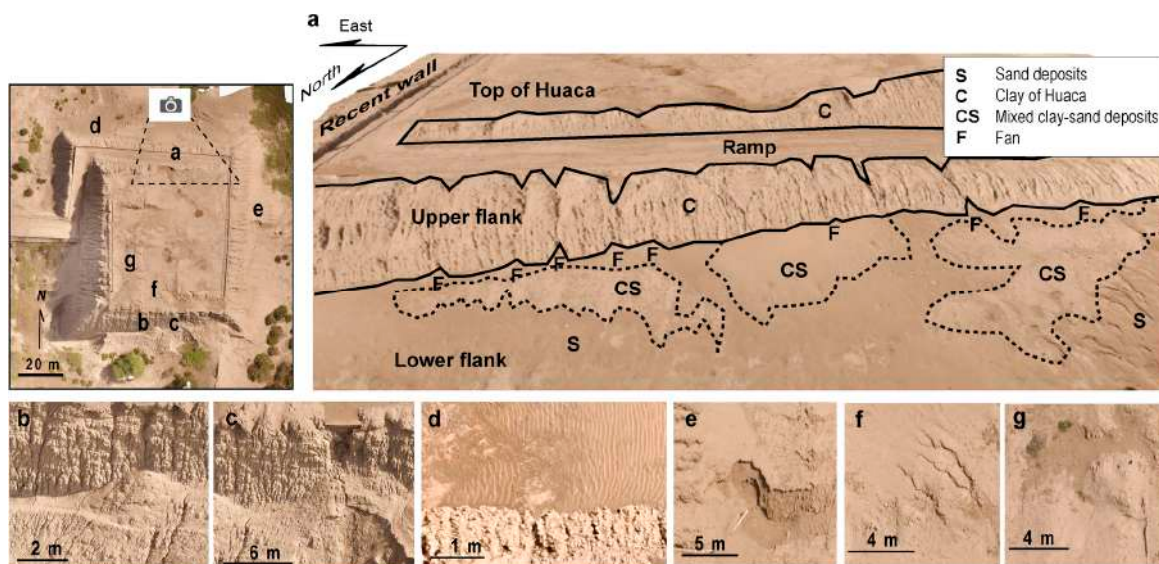


Figure 4. Top left: Orthophoto of the Huaca Chotuna with location of the images reported in (a–d). (a) Panoramic view of the northern sector with specifications of the areas covered by different deposits. (b) Fan-like structure develops at the mouth of an incision (gully). (c) Slide scar affecting the lower southern flank. (d) Ripple sedimentary structures at the base of the northern flank. (e) Morphological depression produced by regressive erosion by water flowing in a drainage tube (white tube). (f) Sub-parallel incision on the top of the Huaca Chotuna. (g) Morphological depression and brush on the top of the Huaca Chotuna.

The results of the field and photogrammetric also evidence larger-scale structures related to deposition or erosion phenomena (Figure 4). The upper flanks of the HC consist of clay-rich deposits derived from the dismantling of the underlying adobes and are affected by parallel incisions (gullies) evidencing erosion by water (Figure 4a). The spacing among the incisions is in the order of dm-m. The HC lower flanks consist of loose, massive sands and mixed clay-sand sediments possibly reflecting mixing between the clay from the dismantled bricks and the sands forming the substratum on which the HC has been constructed. At the mouth of the main incisions, fan-like structures and sedimentary wedges (Figure 4a,b) may occur. Some wedges are partially collapsed as testified by slide scars (Figure 4c). Roughly N-S striking ripples due to the wind action outcrop at the base of the northward- and southward-dipping lower flanks of the HC (Figure 4d). The undulation of such ripples, which consist of sand, shows a slight, east-verging asymmetry. At the base of the western flank, we also recognize a 1.5 m deep channel with an east-verging head (Figure 4e). The field survey and orthophotos show that the water discharged from a drainage tube is responsible for the formation of this channel. The top of the HC is also affected by erosive structures. These include up to 8 m long converging incisions (Figure 4f) and two elongated depressions covering an area of 16 m². Such depressions do not exceed 1 m in depth. They are partially filled with sand and may host a few shrubs, the only variety of vegetation on the HC (Figure 4g).

4.2. Spatial Distribution of the Morphometric Parameters

The results of the quantitative parameters extracted from the analysis of the DSM are reported in Figures 5–9. We perform a quantitative analysis of the gullies affecting the upper and lower flanks of the HC using a DSM and determine their average spacing (distance between gullies), depth, and variation range (difference between the maximum and minimum altitude of the gullies along the profile). The results show that the average spacing of the north-dipping flank is 1.25 m⁻¹ and that of the south-dipping flank is 1.34 m⁻¹. The east-dipping and west-dipping flanks have values of 0.88 m⁻¹ and 0.89 m⁻¹, respectively. The depth of the gullies of the northern and southern flanks is 0.15 m and 0.34 m, respectively, while that of the eastern and western flanks is 0.75 m and 0.98 m, respectively. Data from Figure 5 reveal that the range of values of the northern (profile 1) and southern flanks (profiles 3 and 4) are significantly lower than those of the eastern (profile 2) and western (profile 5) flanks. In summary, the above summarized data show that the eastern and western flanks are characterized by lower values of spacing with respect to the northern and southern flanks but by higher values of depth of gullies and range.

The spatial distribution of slope (Figure 6a,b) defines the main geomorphic structure of the HC and the surrounding area. The top of the HC, the ramp, and the areas outside the main construction show slope values < 20° while the lower flanks have slopes between 20° and 42°. The upper flanks have slope values of >42°. The distribution of the aspect values shows three main peaks at 90° (east), 180° (south), and 270° (west) (Figure 6c,d). The lack of a well-defined peak of a north-facing slope in the distribution of the aspect values is due to the larger amount of sediments mantling the northern flank of the HC with respect to the other flanks, which are less affected by a sedimentary cover. However, data from Figure 6e evidence four main peaks at north, south, east, and west for slope values of >42°, i.e., the upper flanks of the HC. This implies that the upper flanks of the huaca are representative of the architectural layout, including the original slope and aspect range of the values. Figure 6e also shows that the main geomorphic structure of the HC may be defined on the basis of the altitude and aspect values with the lower flanks developing between 13 m and 23 m and the upper flanks between 23 and 31 m.

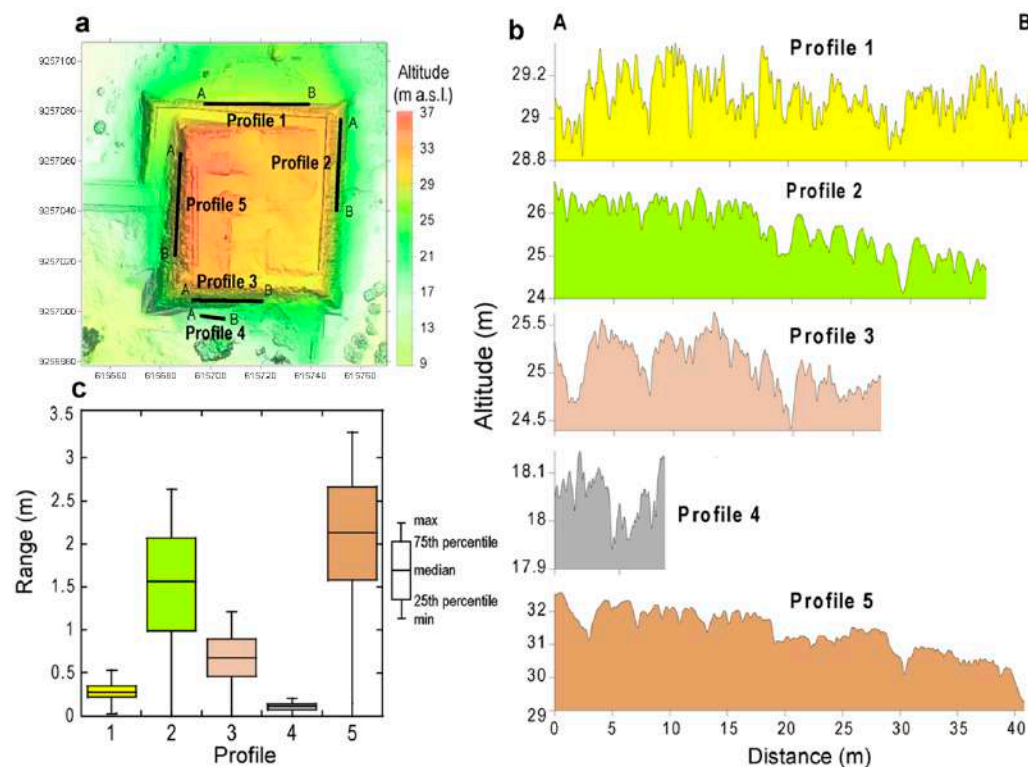


Figure 5. (a) DSM of the Huaca Chotuna with location of the morphological profiles reported in (b). (b) Morphological profiles along the flanks of the Huaca Chotuna. Box plot of the range values determined from each morphological profile reported in (c). Range is the difference between the altitude values along a profile and the minimum value of the profile.

The geometry of the stream network and associated watershed basins is controlled by the HC architectural layout with sub-parallel, low Strahler-order drainage affecting the upper and lower flanks (Figure 7a). The top of the HC is characterized by a more complex drainage with two higher Strahler-order main channels with an average NW-SE strike. This indicates that the drainage at the HC top is due to a south-east-facing surface with slope values lower than about 8° (Figure 6a,c). The modern walls delimiting the access ramp and the eastern side of the HC top act as channel boundary regimenting the local water flow. The values of TWI are consistent with the above-described picture (Figure 7b). The areas of the HC where the water may flow or stagnate during rainfall episodes concentrate at the top and on the access ramp. Along the flanks, the water flows in sub-parallel rills and tends to accumulate and stagnate in areas surrounding the HC architectural structure. Also, we note a notable E-W striking water flow zone departing from the southeastern corner of the top of the HC and propagating eastward on the eastern flank. The water flowing from a drainage tube located just below a wall at the western tip of such water flow zone (Figures 2b and 7a,b) may be responsible for the formation of a well-incised channel in which flow concentrates.

The spatial distribution of the O_f values indicates that the larger distance covered by the flowing water is expected to occur along the flanks of the HC (Figure 7c), a feature consistent with the higher slope values of the HC upper flanks with respect to those of the lower flanks and the HC top (Figure 6a,b,e). Therefore, the north-, east-, south-, and west-facing slopes are expected to be sites where the distance covered by the water flow outside the HC is maximized (Figure 7d).

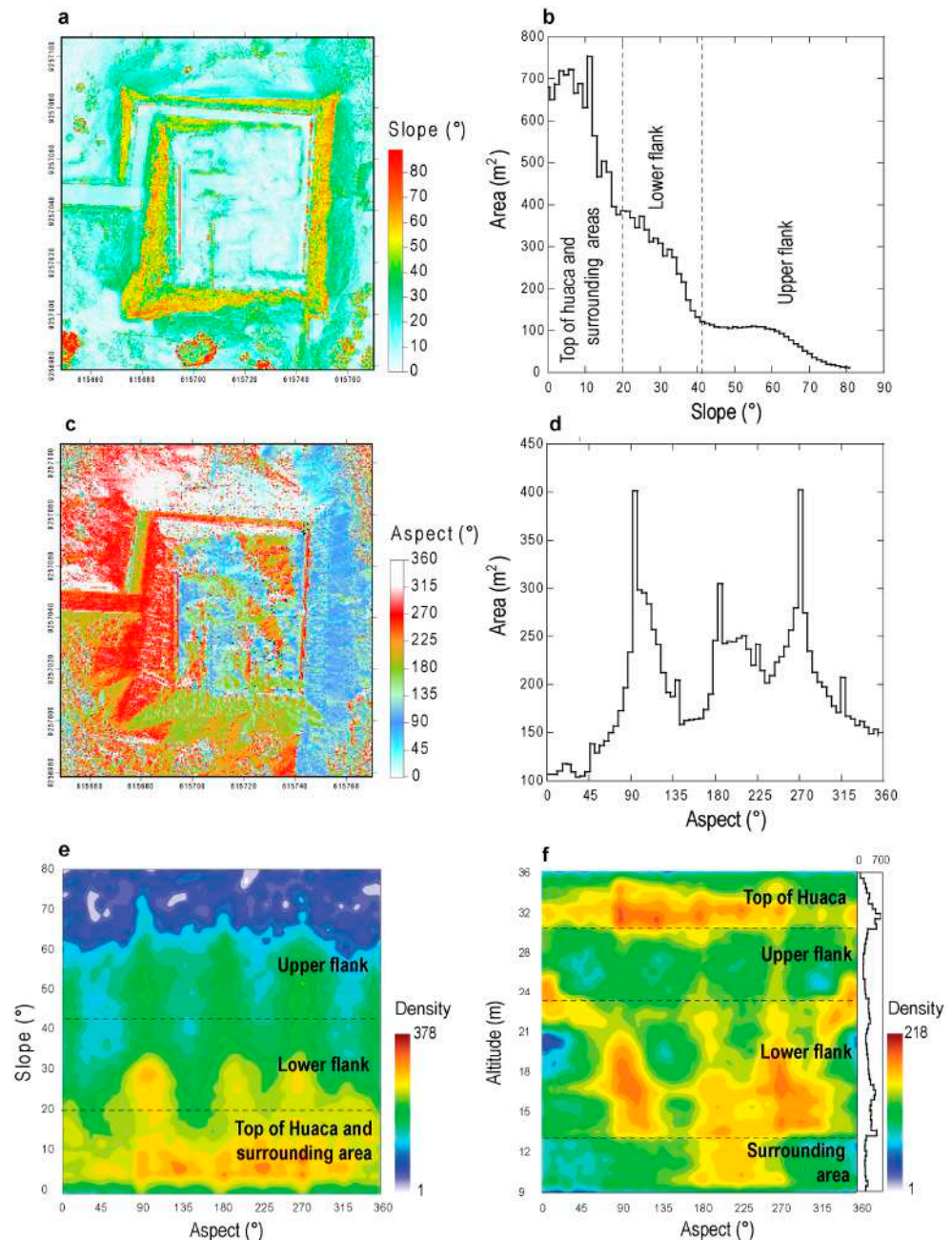


Figure 6. (a) Slope map of the Huaca Chotuna obtained from the DSM. (b) Histogram of the distribution of the slope values. (c) Aspect map of the Huaca Chotuna obtained from the DSM. (d) Histogram of the distribution of the aspect values. (e) Density plot of the aspect vs. slope values from the DSM. (f) Density plot of the aspect vs. altitude values from the DSM.

The HC sectors with the larger exposure to the winds from the south, i.e., those related to the Humboldt current, are shown in Figure 8a. The sector with WEI values of >1.10 is the southern flank while the WEI values between 1 and 1.10 characterize the northern lower flank, and the southern half of the eastern and western lower flanks. The northern upper flanks and the northern half of the eastern and western flanks are downwind with a WEI of <1 . The top of the HC is characterized by a WEI of generally <1 with very few areas with values up to 1.05. The HC sectors with an upwind exposure to the winds from the west, i.e., those related to the ENSO events, are reported in Figure 8b. The sectors with a WEI of >1.10 are the western lower flank and the lower access ramp. The northern, southern, and eastern flanks have a WEI between 1 and 1.05 except for the east-dipping, uppermost

flank, which has a WEI of <1. The HC top is characterized by upwind and downwind areas with a WEI between 0.95 and 1.05.

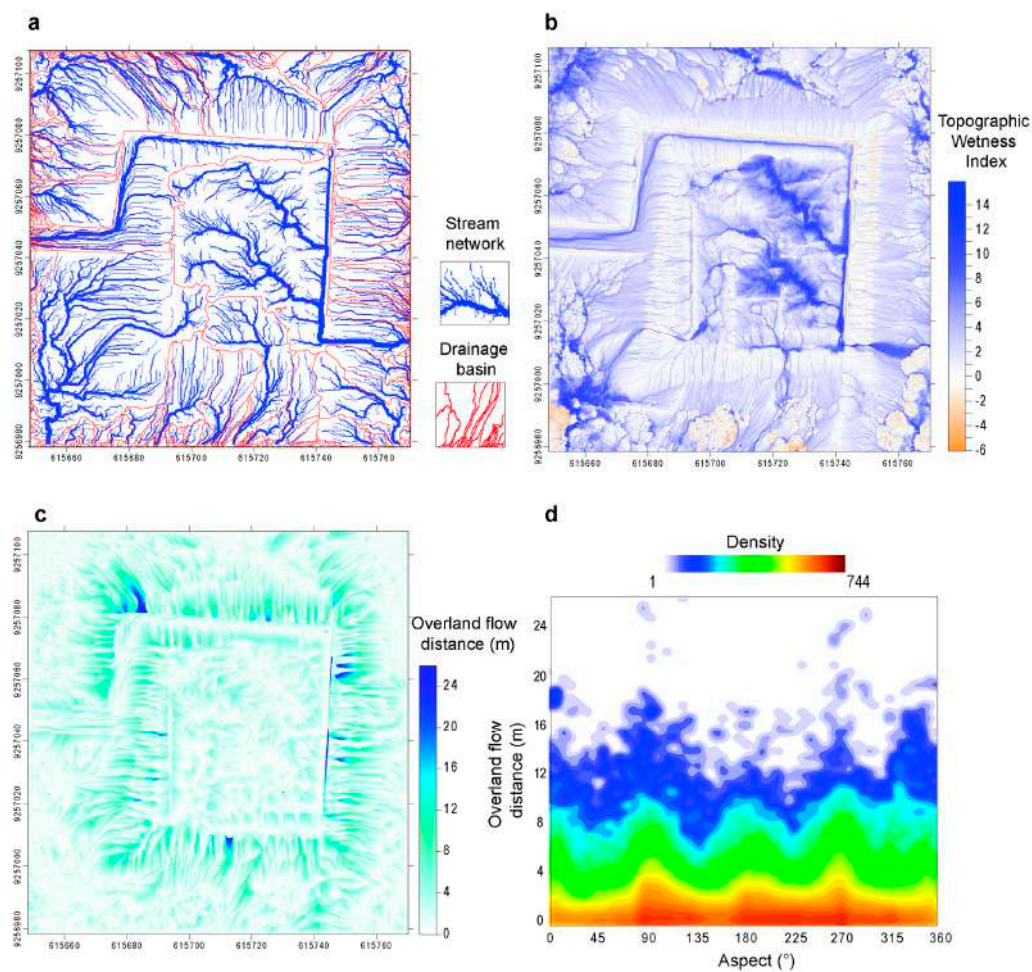


Figure 7. (a) Stream network and drainage basins map of the Huaca Chotuna obtained from the DSM. Stream thickness proportional to the Strahler-order (b) TWI map of Huaca Chotuna. (c) Overland flow distance map of the Huaca Chotuna. (d) Density plot of the aspect vs. overland flow distance obtained from the maps in Figures 6c and 7a.

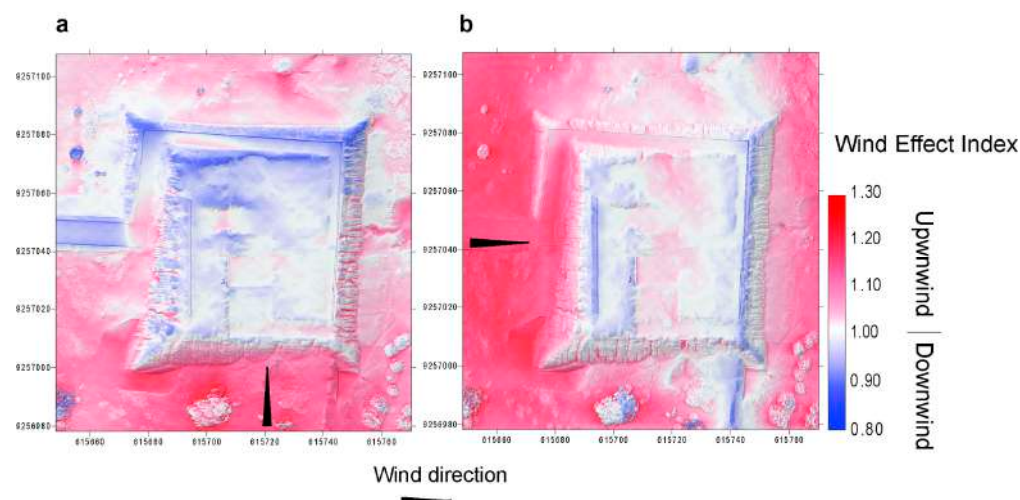


Figure 8. Spatial distribution of the wind effect index values on the Huaca Chotuna in the case of winds from the south (a) and from the west (b).

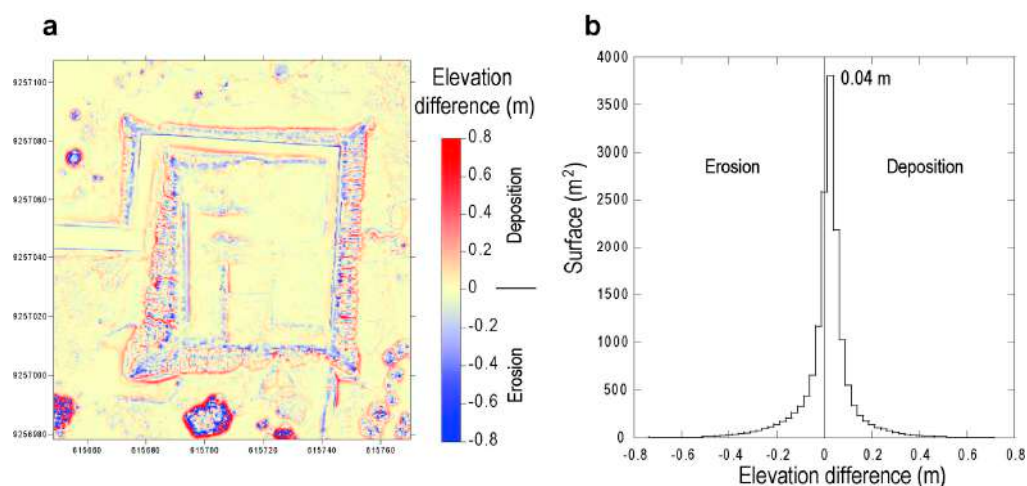


Figure 9. (a) Results of a diffusion model over a period of 1 century showing the areas potentially affected by erosion and deposition. (b) Histograms and maximum value of the data reported in (a).

Figure 9a,b reports the HC areas where erosion or deposition from diffusive processes are likely to occur in the next century. Independently from the calculated elevation difference, which may be dependent on the selected value of the diffusion coefficient (see Equation (6)), the areas of erosion or deposition are well-defined. The base of the HC flanks and the incisions associated with gully erosion are sites where deposition is expected to occur. Erosion concentrates on the present-day topographically elevated elements such as the modern walls and remnants of the ancient walls at the HC top.

The northwestern, northeastern, southeastern, and southwestern HC corners, which represent architectural elements where the orthogonal HC flanks converge, are also sites of potential erosion as well as the natural divides of the main gullies. Figure 9b shows that the surface covered by sedimentation processes is slightly greater than that potentially affected by erosion. An analysis of Figure 9a reveals that most of the sedimentation processes will concentrate at the base of the HC flanks, where the present-day fans cluster (Figure 4a,b).

5. Discussion

The field data collected on the HC platform reveal that this archaeological structure is made up of adobes with a shape (loaf and tall loaf) ascribable, according with the classification by [22,48], to the Classic Lambayeque (12th–14th Century AD), and Late Lambayeque, Chimú-Inca and Inca (14th–16th Century AD). The analysis of the orthophotos, DSM, and morphometric parameters and direct observations show that the HC is affected by erosion and sedimentation processes. Although the results of our analysis are based on a DSM with a centimeter resolution, the extracted morphometric parameters have a decimeter resolution. This limits our interpretation to a decimeter to meter scale, preventing a detailed analysis of the erosion and deposition processes at a smaller scale. Therefore, our approach is unable to quantify (a) the erosive processes affecting individual bricks and (b) the sedimentation processes by sediment-laden winds on restricted areas around or above HC. Also, our theoretical estimate of the areas potentially affected by erosion or deposition processes based on the diffusion model are limited by the assumption that the diffusion coefficient is assumed to be constant with time. All the above-mentioned limitations should be considered in the approach we have proposed and in the discussion of the results.

5.1. Erosion Processes, Associated Hazard, and Precautionary Measures

Erosion is testified by the gully-type incisions recorded on the upper and lower flanks. These incisions define a parallel drainage network, which, according to [64,65], form by water erosion on constant slope surfaces with a homogeneous lithology. These latter conditions are fully satisfied on the HC flanks. Because of the semi-arid conditions of the Lambayeque coast, we propose that the water flow responsible for the erosion of the HC flanks is due to rain related to the ENSO events, which are characterized by winds from the west [36]. This interpretation is supported by the data on the gully depth, which reaches its maximum value (0.98 m) on the western HC flank. Assuming that the HC has not been restructured from the 16th Century AD (Spanish conquest) and taking into account the above reported maximum value, we estimate a maximum vertical erosion rate of about 0.2 m/century. This value is about ten times the maximum value estimated for the erosion rate of sedimentary rocks in arid environments (0.01 m/century), or drainage basins (0.02 m/century; [66]), and of the same order of magnitude to that calculated for the vertical incision rate of rivers (0.2–0.3 m/century; [67]). Therefore, we conclude that the preservation potential of the HC is very low, mainly due to the erosion by rainwater during the ENSO events. Although a quantification of the effects of single, heavy rain episodes or seasonal, ENSO-related episodes on the HC bricks cannot be quantified based on the available data, our estimate of the vertical erosion rate suggest that a single HC brick, which is 15 to 20 cm thick, if totally exposed to weathering, may be fully eroded on a time scale of 0.75–1.0 century.

The statistical distribution of the range values along the HC flanks shows that, with respect to the eastern, southern, and northern flanks, the western flank is characterized by the larger variation range (3.3 m) and highest median value (2.1 m; Figure 5c). Therefore, we conclude that rain associated with the ENSO events is responsible for most of the erosive features affecting the HC. Rain is also responsible for the partial/total melting of the HC adobes and for the water–clay mixture (mud) forming the clay-rich patina covering the underlying bricks (Figure 3c). Evidence of water-related erosion also characterizes the HC top, where converging incisions and elongated depressions are recognized (Figure 4f,g). Because of the low slope values of the HC flat top (Figure 6f), these incisions and depressed areas are significantly less developed with respect to those affecting the flanks. However, the TWI and O_f maps suggest that these depressed areas represent zones of prevailing water stagnation more than water flow (Figure 7b,c), a feature consistent with the occurrence of brush within such zones. Erosion due to anthropic activity characterizes the eastern sector of the HC with up to 1.5 m deep incisions developing in an area where the water from drainage tubes has eroded the deposits of the HC lower flank (Figures 2b and 4e). These incisions are characterized by retrogressive (upstream) erosion [68], a process favored by the high slope of this one and lower slopes of the HC lower flanks deposits. As a result, we propose extending these drainage tubes to flat areas located away from the HC and from the sediments on the lower flanks. Otherwise, retrogressive erosion processes could propagate upstream with time affecting the whole lower and upper HC flanks. The spatial distribution of the overland flow distance (Figure 7c) around the HC reveals that water flows may propagate outside the HC perimeter at distances up to about 20–25 m during rain episodes. Therefore, we suggest scheduling a 30–40 m wide buffer zone around the HC during the ENSO events to reduce the hazard related to possible, intense water flows. This is also for the northern and southwestern areas surrounding the HC and the access ramp. Here, even though the overland flow distance decreases, coalescing streams may locally increase the water flow during rain episodes (Figure 7a,b). The occurrence of slide scars at the top of the southern lower flank and at the southeastern corner of the platform testifies a landslide hazard affecting the HC flanks. For this reason, the access to the areas

surrounding the HC should not be allowed being the quantitative estimate of the landslide hazard is problematic, mainly for the restricted area (few square meters) of the potentially affected surface. In summary, the water-related to rain episodes during the ENSO events and gravity processes pose a problem of hazard at the HC. Based on the above discussed data, the whole HC structure and surrounding areas should not be accessible during intense rain episodes, whereas the access ramp and the top are relatively safe during the dry season. The lower and upper HC flanks are, on the contrary, unsafe areas because sites of potential gravity phenomena and water/mud flows during rain.

5.2. Sedimentation Processes and Preservation Actions

The evidence of active sedimentation processes at the HC occurs on the lower flanks, which are made up of aeolian sand deposits. Such deposits mask the original flanks of the HC up to about half of the HC height (Figures 2a and 3a–c). Data from Figure 4d show slightly asymmetric eastward verging ripples indicating prevailing winds from the west. According to the results on the distribution of the WEI in Figure 8, all the HC flanks show an exposure to winds from the south (Humboldt current), and from the west (ENSO events). Therefore, while the accumulation of sand by aeolian processes on the HC flanks may occur all year, the ripples found at the HC record probably formed during the last ENSO event between February and April 2025. This implies that air currents affecting the HC favor sediment-laden winds, which represent the climatic process responsible for the partial burial of the platform. These winds are also responsible for the limited sand-filling of the depressed areas at the top of the HC (Figure 4g). A further sign of active sedimentation process at the HC is the occurrence of clay or mixed sand–clay fan-like structures found at the base of the upper flanks (Figure 4a,b). These fans, located at the mouth of the sub-parallel gullies affecting the HC upper flanks, easily form by gravity processes because their maximum slope is 30° – 35° , a value less than the slope of the upper flanks ($>42^{\circ}$), and close to the repose angle of dry sand with rounded particles and dry clay (34 – 35° ; [69,70]).

The simulation of sedimentation or erosion by diffusion processes for the next century summarized in Figure 9a,b does not consider the contribution of sediment-laden winds. However, the area of deposition is larger than that of erosion. This result implies that the HC platform will be subjected to prevailing material accumulation processes, mainly concentrated at the base of the upper flanks. Therefore, the HC architectural structure is expected to be gradually obscured by addition of clay and sand, also in the absence of winds. Such material comes from the dismantling of the uppermost, subvertical slopes at the top of the upper flanks and, in a less amount, from the material moving down within the gully-type incisions. Also, these latter are expected to deepen by water washing erosion and during the ENSO events. In this picture, the HC must be protected from the effects of long-term diffusion processes. We propose to cover the whole HC structure with impermeable material, a solution also adopted in other huacas, e.g., the Huaca I at Tucume (<https://www.wmf.org/projects/t%C3%BAcume-archaeological-site>, accessed on 15 May 2025), and the Huaca de Moche at Trujillo (<https://huacasmoches.pe/proyecto-arqueologico/>, accessed on 15 May 2025). At the HC, waterproofed wood could be used. The seasonal removal of sand accumulated by sediment-laden winds above the flanks could also be implemented to preserve the HC architectural structure.

The above discussed results show that rainfall and winds are mainly responsible for the deterioration of the HC clay structure and pose a significant hazard. The occurrence of gravity slides also highlights a problem of structural integrity of the HC platform. While rain, which mainly concentrates during the ENSO events between February and March, affects the HC flanks triggering gully erosion processes, sediment-laden winds tend to bury the structure. These winds occur during the whole year, although their intensity

increases during the ENSO events. Because the frequency and intensity of these events are expected to rise in the future due to climate change [27], erosive and burial processes are also expected to increase. The interdisciplinary approach we propose in this study and the recognized hazard(s), are relevant not only for the evaluation of the degree of preservation of other huacas in Peru but also for the study of the effects of erosive and burial processes related to the climate change on other earthen archaeological sites worldwide, which represent about 10% of the world's heritage, as previously reported [19]. Studies focusing on erosion/deposition processes in archaeological contexts like that proposed here should be inserted and implemented in quantitative analyses focused on land use and natural hazard mitigation strategies, as well as for the implementation of conservation plans of cultural heritage [71,72].

6. Conclusions

The combined analysis of a DSM, orthophotos, and extracted morphometric parameters reveals that the HC is affected by erosive, deposition, and gravity processes due to different triggering mechanisms. Erosive processes due to water flow are related to rain during the ENSO events and mainly concentrate on the HC flanks. Gully erosion produces parallel incisions on the HC flanks with an estimated vertical erosion rate of about 0.2 m/century. Morphological structures of retrogressive erosion due to anthropic drainage activity are also recognized. Sediment-laden winds are responsible for the burial of half of the HC flanks. We recognize two main wind directions: (a) winds from the south originating from the Humboldt current during the whole year and (b) winds from the west concentrated during the ENSO episodes between the February–April period. Ripple asymmetry indicates the present-day action of ENSO-related winds. Gravity sliding processes also affect the HC flanks and may potentially reduce the structural and architectural integrity of the HC flanks in the future.

The relevant hazards documented at the HC may be reduced by adopting some solutions aimed at preserving the structure from the action of wind (wind barriers) and rainfall (impermeable cover). The creation of buffer zones in which the access is limited is also proposed. However, a specific study aimed at implementing a conservation plan should be carried out by merging data from this study archaeological and architectural/engineering investigations.

In this study, we show that the morphometric analysis of sites and the coupling of quantitative parameters and climatic data provide a useful tool to identify the natural processes responsible for the deterioration of the structures. Also, the application of diffusion models may allow the identification of areas subjected to future erosion or sedimentation (deposition) processes. Our analytical approach could be extended to other earthen archaeological sites affected by rain, wind, and gravity instability with the aim to recognize the exposure to natural hazard(s). Future trends should include the evaluation of the increasing intensity of potentially dangerous and/or damaging natural phenomena due to climate change on ancient remains by merging historical, morphological, climate, and engineering/architectural information in physically based models.

Author Contributions: Conceptualization, G.V.; methodology, L.M. and G.V.; formal analysis, L.M., G.V., M.I.P.A. and R.F.G.C.; resources, M.I.P.A., M.F.M. and C.E.W.L.T.; data curation, G.V. and R.F.G.C.; writing—original draft preparation, M.I.P.A. and G.V.; writing—review and editing, L.M., G.V. and M.I.P.A.; visualization, L.M. and G.V.; supervision, G.V.; project administration, M.I.P.A., C.E.W.L.T. and M.F.M.; funding acquisition, L.M., M.I.P.A., C.E.W.L.T. and M.F.M. All authors have read and agreed to the published version of the manuscript.

Funding: This research was supported by internal funds of the Istituto Nazionale di Geofisica e Vulcanologia (Roma1 section), Italy, within the activities of the project Arch3023 2025 'Huacas' accredited by Ministero degli Affari Esteri e della Cooperazione Internazionale of Italy to Maria

Ilaria Pannaccione Apa". This study was produced with co-funding from the European Union—Next Generation EU—Project ID Code PE_0000020 "CHANGES—Cultural Heritage Active Innovation for Sustainable Society," CUP H53C22000850006. This manuscript reflects only the authors' views and opinions; neither the European Union nor the European Commission can be considered responsible for them.

Data Availability Statement: Data of this article are subjected to embargo due to legal restrictions of the Ministry of Culture of Peru.

Acknowledgments: We thank the colleagues at INGV and Museo Arqueológico Nacional Brüning for discussions.

Conflicts of Interest: The authors declare no conflicts of interest.

References

1. Agapiou, A.; Lysandrou, V.; Hadjimitsis, D.G. A European-Scale Investigation of Soil Erosion Threat to Subsurface Archaeological Remains. *Remote Sens.* **2020**, *12*, 675. [\[CrossRef\]](#)
2. Borrelli, P.; Robinson, D.A.; Panagos, P.; Lugato, E.; Yang, J.E.; Alewell, C.; Wuepper, D.; Montanarella, L.; Ballabio, C. Land use and climate change impacts on global soil erosion by water (2015–2070). *Proc. Natl. Acad. Sci. USA* **2020**, *117*, 21994–22001. [\[CrossRef\]](#)
3. Emberson, R.A. Dynamic rainfall erosivity estimates derived from IMERG data. *Hydrol. Earth Syst. Sci.* **2023**, *27*, 3547–3563. [\[CrossRef\]](#)
4. Grillakis, M.G.; Polykretis, C.; Alexakis, D.D. Past and projected climate change impacts on rainfall erosivity: Advancing our knowledge for the eastern Mediterranean island of Crete. *Catena* **2020**, *193*, 104625. [\[CrossRef\]](#)
5. Wynants, M.; Kelly, C.; Mtei, K.; Munishi, L.; Patrick, A.; Rabinovich, A.; Nasseri, M.; Gilvear, D.; Roberts, N.; Boeckx, P.; et al. Drivers of increased soil erosion in East Africa's agro-pastoral systems: Changing interactions between the social, economic and natural domains. *Reg. Environ. Change* **2019**, *19*, 1909–1921. [\[CrossRef\]](#)
6. Adeyeri, O.E.; Folorunsho, A.H.; Adeliyi, T.E.; Ayegbusi, K.I.; Akinsanola, A.A.; Ndehedehe, C.E.; Ahmed, N.; Babalola, T.E. Climate change is intensifying rainfall erosivity and soil erosion in West Africa. *Sci. Total Environ.* **2024**, *955*, 177174. [\[CrossRef\]](#)
7. Panagos, P.; Borrelli, P.; Meusburger, K.; Yu, B.; Klik, A.; Jae Lim, K.; Yang, J.E.; Ni, J.; Miao, C.; Chattopadhyay, N.; et al. Global rainfall erosivity assessment based on high-temporal resolution rainfall records. *Sci. Rep.* **2017**, *7*, 4175. [\[CrossRef\]](#)
8. Orr, S.A.; Young, M.; Stelfox, D.; Curran, J.; Viles, H. Wind-driven rain and future risk to built heritage in the United Kingdom: Novel metrics for characterising rain spells. *Sci. Total Environ.* **2018**, *640*, 1098–1111. [\[CrossRef\]](#)
9. Harkin, D.; Davies, M.; Hyslop, E.; Fluck, H.; Wiggins, M.; Merritt, O.; Barker, L.; Deery, M.; McNeary, R.; Westley, K. Impacts of climate change on cultural heritage. *MCCIP Sci. Rev.* **2020**, *16*, 24–39.
10. Sesana, E.; Gagnon, A.S.; Ciantelli, C.; Cassar, J.; Hughes, J.J. Climate change impacts on cultural heritage: A literature review. *WIREs Clim. Change* **2021**, *12*, e710. [\[CrossRef\]](#)
11. Magnini, L.; Pozzi-Escot, D.; Oshiro, J.; Angeles, R.; Apa, M.I.P.; Ventura, G. Effects of the Architectural Layout of the Sanctuary of Pachacamac (2nd–16th Century CE, Peru) on the Exposure to Rain, Wind, and Solar Radiation from the Morphometric Analysis of Digital Surface Models. *Remote Sens.* **2024**, *16*, 1848. [\[CrossRef\]](#)
12. Yeh, S.W.; Kug, J.S.; Dewitte, B.; Kwon, M.-O.; Kirtman, B.P.; Jin, F.-F. El Niño in a changing climate. *Nature* **2009**, *461*, 511–514. [\[CrossRef\]](#)
13. Daly, C.; Purcell, C.E.; Donnelly, J.; Chan, C.; MacDonagh, M.; Cox, P. Climate change adaptation planning for cultural heritage, a national scale methodology. *J. Cult. Herit. Manag. Sustain. Dev.* **2021**, *11*, 313–329. [\[CrossRef\]](#)
14. Kapsomenakis, J.; Douvis, C.; Poupkou, A.; Zerefos, S.; Solomos, S.; Stavvaka, T.; Melis, N.S.; Kyriakidis, E.; Kremlis, G.; Zerefos, C. Climate change threats to cultural and natural heritage UNESCO sites in the Mediterranean. *Environ. Dev. Sustain.* **2022**, *25*, 1–26. [\[CrossRef\]](#)
15. UNESCO. *Climate Change and World Heritage. Report on Predicting and Managing the Impacts of Climate Change on World Heritage and Strategy to Assist States Parties to Implement Appropriate Management Responses*; UNESCO World Heritage Centre: Paris, France, 2007.
16. Sabbioni, C.; Brimblecombe, P.; Cassar, M. *The Atlas of Climate Change Impact on European Cultural Heritage: Scientific Analysis and Management Strategies*; Anthem Press: London, UK, 2010.
17. Xiao, W.; Mills, J.; Guidi, G.; Rodríguez-González, P.; Gonizzi Barsanti, S.; González-Aguilera, D. Geoinformatics for the Conservation and Promotion of Cultural Heritage in Support of the UN Sustainable Development Goals. *ISPRS J. Photogramm. Remote Sens.* **2018**, *142*, 389–406. [\[CrossRef\]](#)

18. Vandemeulebroucke, I.; Kotova, L.; Caluwaerts, S.; van Den Bossche, N. Degradation of brick masonry walls in Europe and the Mediterranean: Advantages of a response-based analysis to study climate change. *Build. Environ.* **2023**, *230*, 109963. [CrossRef]
19. Gandreau, D.; Delboy, L. *World Heritage: Inventory of Earthen Architecture*; CRATerre-ENSAG: Grenoble, France, 2012; pp. 1–284. ISBN 978-2-906901-70-4.
20. Mileto, C.; López-Manzanares, F.V. Earthen architectural heritage in the international context: Values, threats, conservation principles and strategies. *J. Cult. Herit. Manag. Sustain. Dev.* **2022**, *12*, 192–205. [CrossRef]
21. Cieza de León, P. *Crónica del Perú Primera Parte*; Original Work Published 1553; Pontificia Universidad Católica del Perú: Lima, Peru, 1984. [CrossRef]
22. Donnan, C. En busca de Naylamp: Chotuna, Chornancap y el valle de Lambayeque. In *Lambayeque*; De Lavalley, J.A., Ed.; Banco de Crédito del Perú: Lima, Peru, 1989; pp. 105–136.
23. Sandweiss, D.H.; Maasch, K.A.; Richardson, J.B.; Rollins, H.B.; Clement, A. Variation in Holocene El Niño frequencies: Climate records and cultural consequences in ancient Peru. *Geology* **2001**, *29*, 603–606. [CrossRef]
24. Chambí, V.; Paula, S.; Zubiato, O.; Beltzadit, M.; Juárez, N.; Segundo, P.; Pinto, P.; Walter. *Riesgo Geológico en la Región Lambayeque. Boletín 43*; Instituto Geológico, Minero y Metalúrgico—INGEMMET: Lima, Peru, 2010; Available online: <https://repositorio.ingemmet.gob.pe/handle/20.500.12544/248> (accessed on 30 June 2025).
25. Oerder, V.; Colas, F.; Echevin, V.; Codron, F.; Tam, J.; Belmadani, A. Peru-Chile upwelling dynamics under climate change. *J. Geophys. Res. Ocean.* **2015**, *120*, 1152–1172. [CrossRef]
26. L’Heureux, M.L.; Tippett, M.K.; Takahashi, K.; Barnston, A.G.; Becker, E.J.; Bell, G.D.; Di Liberto, T.E.; Gottschalck, J.; Halpert, M.S.; Hu, Z.-Z.; et al. Strength Outlooks for the El Niño-Southern Oscillation. *Weat. Forecast.* **2019**, *34*, 165–175. [CrossRef]
27. Geng, T.; Cai, W.; Jia, F.; Wu, L. Decreased ENSO post-2100 in response to formation of a permanent El Niño-like state under greenhouse warming. *Nat. Commun.* **2024**, *15*, 5810. [CrossRef]
28. Vuille, M.; Southon, J. Climate change and El Niño variability in the Peruvian Andes: Insights from paleoclimate records. *Quat. Sci. Rev.* **2009**, *28*, 3001–3012.
29. McGregor, H.V.; Fischer, M.J.; Gagan, M.K.; Fink, D.; Phipps, S.J.; Wong, H.; Woodroffe, C.D. A weak El Niño/Southern Oscillation with delayed seasonal growth around 4,300 years ago. *Nat. Geosci.* **2013**, *6*, 949–953. [CrossRef]
30. Ortloff, C.R.; Kolata, A.L. El Niño and the ancient civilizations of Peru. *Geoarchaeology* **1993**, *8*, 415–428.
31. DeFrance, S.D.; Sandweiss, D.H.; Richardson, J.B. Early adaptation to El Niño in coastal Peru during the mid-Holocene. *Proc. Natl. Acad. Sci. USA* **2015**, *112*, 12651–12656.
32. Delle Rose, M. Landscape Modifications Ascribed to El Niño Events in Late Pre-Hispanic Coastal Peru. *Land* **2022**, *11*, 2207. [CrossRef]
33. Moseley, M.E. El Niño and the collapse of the Moche civilization. In *El Niño and the Southern Oscillation: Multiscale Variability and Global and Regional Impacts*; Diaz, H.F., Markgraf, V., Eds.; Cambridge University Press: Cambridge, UK, 2001; pp. 461–481.
34. García, A.; Takahashi, K.; Espinoza, J.C.; Lavado-Casimiro, W.; Sulca, J.; Carbajal, L. Socioeconomic impacts of El Niño in northern Peru: Historical and modern perspectives. *J. Lat. Am. Geogr.* **2012**, *11*, 123–144.
35. Bayer, A.M.; Danysh, H.E.; Garvich, M.; González, G.; Checkley, W.; Alvarez, M.; Gilman, R.H. An unforgettable event: A qualitative study of the 1997–98 El Niño in northern Peru. *Disasters* **2014**, *38*, 351–374. [CrossRef]
36. Peng, Q.; Xie, S.-P.; Passalacqua, G.A.; Miyamoto, A.; Deseret, C. The 2023 extreme coastal El Niño: Atmospheric and air-sea coupling mechanisms. *Sci. Adv.* **2024**, *10*, eadk8646. [CrossRef]
37. Romero, R.; Takahashi, K.; Espinoza, J.C.; Lavado-Casimiro, W.; Sulca, J.; Carbajal, L. Flood hazards and impacts in the Peruvian coastal region during El Niño episodes. *Nat. Hazards Earth Syst. Sci.* **2009**, *9*, 81–94.
38. Xeres, F. *Verdadera Relación de la Conquista del Perú y Provincia del Cuzco*; Original Work Published 1534; Biblioteca Virtual Miguel de Cervantes: Alicante, Spain, 2011; pp. 1–114. ISBN 978-1466444263.
39. Cieza de León, P. *Crónica del Perú*, Sevilla. 1533. Available online: <https://fuenteshistoricasdelperu.com/2023/04/07/cronica-del-peru-por-pedro-cieza-de-leon-sevilla-1553/> (accessed on 30 June 2025).
40. Cabello Balboa, M. *Miscelánea Antártica*, 29; [1586]; Fundación José Manuel Lara: Lima, Peru, 2011; pp. 1–549. ISBN 8496824810.
41. Alcocer, F. *Probanzas de Indios y Españoles Referencias a las Catastróficas Lluvias de 1578, en los Corregimientos de Trujillo y Saña*; [1578]; Centro de Estudios Sociales Solidaridad: Lima, Peru, 1987; pp. 1–208.
42. Vega de la, G. *Commentari Reali Degli Inca*; [1609]; Bompiani: Milano, Italy, 2011; pp. 1–1024. ISBN 9788858712580.
43. Mackey, C. Los estilos alfareros costeños de los periodos tardíos. In *De Cupisnique a Los Incas*; Castillo, L.J., Pardo, C., Eds.; MALI: Lima, Peru, 2009; pp. 268–303.
44. Shimada, I. *Cultura Sicán: Dios, Riqueza y Poder en la Costa Norte del Perú*; Fundación del Banco Continental para el Fomento de la Educación y la Cultura: Lima, Peru, 1995; pp. 1–226. Available online: https://fundacionbbva.pe/wp-content/uploads/2016/04/libro_000051.pdf (accessed on 30 June 2025).
45. Zevallos Quiñones, J. Introducción a la cultura Lambayeque. In *Lambayeque*; De Lavalley, J.A., Ed.; Banco de Crédito del Perú: Lima, Peru, 1989; pp. 15–103.

46. Wester La Torre, C.E. *Chotuna-Chornancap: Templos, Rituales y Ancestros Lambayeque*; Ministerio de Educación y Unidad Ejecutora 111 Naylamp Lambayeque: Lima, Peru, 2010; pp. 1–252.
47. Wester La Torre, C.E. *Chornancap. Palace of the Leader and Priestess of the Lambayeque Culture*; Ministry of Culture of Perú, EMDECOSEGE.S.A.: Lima, Peru, 2016; pp. 1–422.
48. Donnan, C. *Chotuna and Chornancap: Excavating an Ancient Peruvian Legend*; Cotsen Institute of Archaeology Press, Monograph 70: Los Angeles, CA, USA, 2012; pp. 1–280. [[CrossRef](#)]
49. Brüning, H.E. *Lambayeque Estudios Monograficos*; Dioniso Mendoza Lib. y Casa Editora: Chiclayo, Peru, 1922; pp. 1–206.
50. Kroeber, A.L. *Peruvian Archaeology in 1942*; Viking Fund Publication in Anthropology n. 4. Viking Fund: New York, NY, USA, 1942; pp. 1–151.
51. Pannaccione Apa, M.I.; La Torre, C.W.; Gutierrez Cachay, R.F.; Magnini, L.; Murga, J.C.; Ranera, F.; Ventura, G. Quantitative estimate of the damages from human activities at the Apurlec Monumental Archaeological Complex (seventh–fourteenth century AD, Peru) from multitemporal photogrammetry. *Arch. Anthropol. Sci.* **2023**, *15*, 110. [[CrossRef](#)]
52. Fernandes, N.F.; Dietrich, W.E. Hillslope evolution by diffusive processes: The timescale for equilibrium adjustments. *Water Resour. Res.* **1997**, *33*, 1307–1318. [[CrossRef](#)]
53. Martin, Y. Modelling hillslope evolution: Linear and nonlinear transport relations. *Geomorphology* **2000**, *34*, 1–21. [[CrossRef](#)]
54. Moore, I.D.; Lewis, A.; Gallant, J.C. Terrain Properties: Estimation Methods and Scale Effects. In *Modeling Change in Environmental Systems*; Jakeman, A.J., Ed.; John Wiley & Sons: New York, NY, USA, 1993.
55. Beven, K.J.; Kirkby, M.J. A Physically Based, Variable Contributing Area Model of Basin Hydrology/Un Modèle à Base Physique de Zone d’appel Variable de l’hydrologie Du Bassin Versant. *Hydrol. Sci. Bull.* **1979**, *24*, 43–69. [[CrossRef](#)]
56. Kopecký, M.; Macek, M.; Wild, J. Topographic Wetness Index Calculation Guidelines Based on Measured Soil Moisture and Plant Species Composition. *Sci. Total Environ.* **2021**, *757*, 143785. [[CrossRef](#)]
57. Wang, L.; Liu, H. An Efficient Method for Identifying and Filling Surface Depressions in Digital Elevation Models for Hydrologic Analysis and Modelling. *Int. J. Geogr. Inf. Sci.* **2006**, *20*, 193–213. [[CrossRef](#)]
58. Conrad, O.; Bechtel, B.; Bock, M.; Dietrich, H.; Fischer, E.; Gerlitz, L.; Wehberg, J.; Wichmann, V.; Böhner, J. System for Automated Geoscientific Analyses (SAGA) v. 2.1.4. *Geosci. Model Dev.* **2015**, *8*, 1991–2007. [[CrossRef](#)]
59. Tesema, T.A. Impact of identical digital elevation model resolution and sources on morphometric parameters of Tena watershed, Ethiopia. *Heliyon* **2021**, *7*, e08345. [[CrossRef](#)] [[PubMed](#)]
60. Freeman, G.T. Calculating catchment area with divergent flow based on a regular grid. *Comput. Geosci.* **1991**, *17*, 413–422. [[CrossRef](#)]
61. Böhner, J.; AntoniĆ, O. Land-Surface Parameters Specific to Topo-Climatology, Chapter 8. In *Developments in Soil Science*; Tomislav, H., Hannes, I.R., Eds.; Elsevier: Amsterdam, The Netherlands, 2009; Volume 33, pp. 195–226.
62. Goubanova, K.; Echevin, V.; Dewitte, B.; Codron, F.; Takahashi, K.; Terray, P.; Vrac, M. Statistical Downscaling of Sea-Surface Wind over the Peru–Chile Upwelling Region: Diagnosing the Impact of Climate Change from the IPSL-CM4 Model. *Clim. Dyn.* **2011**, *36*, 1365–1378. [[CrossRef](#)]
63. McKean, J.A.; Dietrich, W.E.; Finkel, R.C.; Southon, J.R.; Caffee, M.W. Quantification of soil production and downslope creep rates from cosmogenic ¹⁰Be accumulations on a hillslope profile. *Geology* **1993**, *21*, 343–346. [[CrossRef](#)]
64. Jung, K.; Niemann, J.D.; Huang, X. Under what conditions do parallel river networks occur? *Geomorphology* **2011**, *132*, 260–271. [[CrossRef](#)]
65. Rhoads, B.L. The Dynamics of Drainage Basins and Stream Networks. In *River Dynamics: Geomorphology to Support Management*; Cambridge University Press: Cambridge, UK, 2020; pp. 15–46.
66. Portenga, E.W.; Bierman, P.R. Understanding Earth’s eroding surface with ¹⁰Be. *GSA Today* **2011**, *21*, 4–10. [[CrossRef](#)]
67. Nativ, R.; Turowski, J.M. Site dependence of fluvial incision rate scaling with timescale. *J. Geophys. Res. Earth Surf.* **2020**, *125*, e2020JF005808. [[CrossRef](#)]
68. Wang, Z.; Xia, J.; Zhou, M.; Deng, S.; Li, T. One-dimensional morphodynamic model for retrogressive erosion based on a sediment entrainment theory at high flow velocity. *Int. J. Sed. Res.* **2021**, *36*, 306–318. [[CrossRef](#)]
69. Al-Hashemi, H.M.B.; Al-Amoudi, O.S.B. A review on the angle of repose of granular materials. *Powder Technol.* **2018**, *330*, 397–417. [[CrossRef](#)]

70. Kim, D.; Nam, B.H.; Youn, H. Effect of clay content on the shear strength of clay–sand mixture. *Int. J. Geo-Eng.* **2018**, *9*, 19. [[CrossRef](#)]
71. Banerjee, R.; Srivastava, P.K. Reconstruction of contested landscape: Detecting land cover transformation hosting cultural heritage sites from Central India using remote sensing. *Land Use Policy* **2013**, *34*, 193–203. [[CrossRef](#)]
72. Guo, H.; Chen, F.; Tang, Y.; Ding, Y.; Chen, M.; Zhou, W.; Zhu, M.; Gao, S.; Yang, R.; Zheng, W.; et al. Progress Toward the Sustainable Development of World Cultural Heritage Sites Facing Land-Cover Changes. *Innovation* **2023**, *4*, 100496. [[CrossRef](#)]

Disclaimer/Publisher’s Note: The statements, opinions and data contained in all publications are solely those of the individual author(s) and contributor(s) and not of MDPI and/or the editor(s). MDPI and/or the editor(s) disclaim responsibility for any injury to people or property resulting from any ideas, methods, instructions or products referred to in the content.